Revision 1 - 8021

Kinetics of dehydrogenation of riebeckite $Na_2Fe^{3+}_2Fe^{2+}_3Si_8O_{22}(OH)_2$: an H*T*-FTIR study

Giancarlo Della Ventura[1,2,3], Francesco Radica[1,2], Federico Galdenzi[1,2], Umberto Susta[1], Gianfelice Cinque[4], Mariangela Cestelli-Guidi[2], Boriana Mihailova[5], Augusto Marcelli[2,6]

1 Dipartimento di Scienze, Università di Roma Tre, L. S. Leonardo Murialdo 1, 00146, Rome
2 INFN-Laboratori Nazionali di Frascati, Via E. Fermi 54, Frascati 00044 (Rome)
3 INGV, Via di Vigna Murata 605, 00143 (Rome)
4 Diamond Light Source Ltd, Harwell Science and innovation Campus, Chilton-Didcot, Oxfordshire OX11 0DE (UK)
5 FB Geowissenschaften, Universität Hamburg, Grindelallee 48, 20146 Hamburg, Germany
6 Rome International Centre for Material Science Superstripes - RICMASS, Via dei Sabelli 119A, 00185 Rome, Italy

Corresponding author:
Giancarlo Della Ventura, Department of Science, University of Roma Tre
Largo S. Leonardo Murialdo 1
00146 Rome (Italy)
giancarlo.dellaventura@uniroma3.it

ABSTRACT

In this work, we address the kinetics of dehydrogenation occurring at high temperatures (HT) in riebeckite, a sodic amphibole with the ideal composition $Na_2Fe^{3+}_2 Fe^{2+}_3Si_8O_{22}(OH)_2$. We did isothermal experiments on both powders and single-crystals up to 560 °C and monitored the O-H stretching signal by Fourier Transform Infrared (FTIR) spectroscopy. Single-crystals show an initial increase in IR absorption intensity due to increasing vibrational amplitudes of the O-H bond stretching, not observed for powders. The OH-intensities *vs.* time were fitted using the formalism for first-order reactions. The calculated activation energies for H^+ diffusion in riebeckite are 159 ± 15 kJ/mol for powders and 216 ± 20 kJ/mol for single

crystals, respectively. The exponential factor *m* in the Avrami-Erofeev equation obtained for crystals ranges between 1.02 and 1.31, suggesting that, unlike powders, the dehydration process in crystals is not a purely first-order reaction. This implies that a second energy barrier must be considered, i.e., diffusion of H^+ through the crystal. FTIR imaging showed that H^+ diffusion occurs mainly perpendicular to the silicate double-chain. Our results confirm that the release of H^+ from riebeckite occurs after the irreversible Fe^{2+}-to-Fe^{3+} exchange, thus at temperatures > 550 °C. To be effective, the process needs the presence of external oxygen that, by interacting with H^+ at the crystal surface, triggers the release of H_2O molecules. This implies that oxidizing conditions are required for the amphibole to be an efficient water source at depth.

KEY WORDS: riebeckite, HT-FTIR spectroscopy, FTIR imaging, Fe-oxidation, dehydration kinetics, activation energy

INTRODUCTION

Dehydration of H_2O/OH-bearing minerals as a function of increasing high temperature/pressure (H*T*/H*P*) conditions is one of the most important processes in geology, being responsible for a wide spectrum of large-scale phenomena such as arc volcanism (e.g. Schmidt and Poli 1998), ore-forming processes (Robb 2005), mantle dynamics and properties (McCammon et al. 2004; Hu et al. 2018), and mantle partial melting (King et al. 2000). Amphiboles, together with layer silicates (Manthilake et al. 2011), play a significant role in this context; they are among the most important hydrous constituents of metamorphic rocks up to H*P* conditions, and are believed to be among the main carriers of water into the mantle during geodynamic processes, considering that they constitute up to 50% by volume of the subduction plate (Christensen and Mooney 1995). Amphiboles have intriguing magnetic (Moukarika et al. 1983; Biedermann et al. 2015) and electrical (Schmidbauer et al. 2000) properties; the latter are enhanced at H*T* and for this reason the amphiboles are believed to play a major role in the conductive anomalies observed in subducted rocks at convergent plate margins (Wang et al. 2012; Hu et al. 2018). Therefore, the detailed knowledge of their stability and transformation processes at high *P*/*T* is mandatory in geological/geophysical research. For Fe-dominant compositions, this task is complicated by the connection between redox phenomena and dehydration/diffusion; the same also occurs at mantle conditions for a variety of Fe-bearing minerals (McCammon et al. 2004). Significant effort was made to define the H*T* stability of sodic Fe-amphiboles of commercial interest ("crocidolite") during the 1960-1970's (Barnes 1930; Addison et al. 1962a, b; Addison and Sharp 1962a, b; Clark and Freeman 1967; Patterson 1964; Hodgson et al. 1964, 1965; Addison and White 1968; Ernst and Wai 1970; Rouxhet et al. 1972), with experiments aimed essentially at defining the Fe oxidation mechanism and the consequent dehydrogenation. Structural adjustments following iron oxidation were later addressed by Ungaretti (1980), Phillips et al. 1988, 1989, 1991) and Popp et al. (1995). Many studies have also focused on the stability of Fe-Ti amphiboles at mantle conditions and the oxo-substitution mechanisms for petrological purposes (King et al. 1999, 2000).

This topic has received renewed interest in recent years thanks to multidisciplinary work on the stability of Fe-rich amphiboles at non-ambient conditions (Welch et al. 2007; Oberti et al. 2016, 2018, 2019; Della Ventura et al. 2018a, b, Mihailova et al., 2021) which showed that the Fe-oxidation – dehydrogenation process is more complicated than that described by the simple equation

$$4Fe^{2+} + 4OH^{-} + {}^{ex}O_2 = 4Fe^{3+} + 4O^{2-} + 2H_2O \qquad (1)$$

In particular, Oberti et al. (2018) and Della Ventura et al. (2018a, b) have recently shown that oxidation/dehydrogenation in riebeckite is a multi-step process, with a temperature range (250 < T < 450 °C) in which Fe oxidation is reversible and followed by a range (450 < T < 550 °C) in which the thermal energy supplied to the system is sufficiently high to trigger expulsion of both electrons and H^+ ions from the surface of the sample. Finally, at T > 550-600 °C, FTIR microspectroscopy shows complete loss of H^+ from the bulk of the crystal and the complete Fe oxidation. Reaction (1) requires the presence of external oxygen ($^{ex}O_2$) (Della Ventura et al. 2018a; Mihailova et al. 2021); where this is the case, H^+ ions are expelled from the amphibole as H_2O molecules at relatively low temperatures compared to other Fe-free/poor amphiboles (consider for example tremolite, where complete OH release occurs after structural collapse at T > 950°C: Johnson and Fegley 2003). This process involves the release of water making amphiboles important carriers of H_2O at depth. It should be emphasized that, owing to this process, riebeckite transforms into an oxo-amphibole, the basic structure topology remaining virtually unchanged, except bond-length and angle adjustments, up to ~900°C. Moreover, Oberti et al. (2018) found that the oxo-amphibole obtained by heating riebeckite had significant ^{A}Na balanced by vacancies at the B- and C-sites, which is in accordance with experimental work showing that sodium amphiboles at high-T in oxidizing conditions deviate in composition towards arfvedsonite (see Ernst 1962 and Della Ventura et al. 2005), The flow of electrons generated during reaction (1) is also responsible for the electrical conductivity observed in the amphibole-bearing rocks heated to HT during subduction (Tolland 1973; Wang et al. 2012; Hu et al. 2018).

A point that needs to be clarified here is the difference between *dehydration* and *dehydrogenation*. Dehydration involves a reaction in which a hydrous phase breaks down for increasing temperature, releases H_2O and transforms into a new mineral, typically in prograde metamorphic reactions. On the other hand, the term dehydrogenation indicates a diffusion and loss of H^+ from the structure without necessarily implying a phase decomposition. Dehydrogenation may occur in Fe- and OH-bearing minerals where the Fe^{2+} to Fe^{3+} conversion for increasing temperature locally balances for the H^+ loss; in such a case the mineral may simply transform into an oxo-counterpart of the starting material, and this is the case of riebeckite studied here. The P-T stability fields and dehydration processes in various amphiboles species have been intensively studied over decades (e.g., Evans 2007; Oberti et al.

2007). However, the process of dehydrogenation at temperatures below the collapse of the amphibole structure is still not completely understood.

In this paper we will address the dehydrogenation mechanism of riebeckite by applying in situ FTIR spectroscopy, in the range of temperatures where the riebeckite – oxo-amphibole transition occurs. We have done isothermal experiments and analysed the behaviour of the O-H bond stretching signal with time. We have used both powders and single crystals to verify the differences between surface and bulk phenomena and to obtain further information on dehydrogenation/oxidation reactions and H^+ diffusion. The anisotropy of the process was additionally monitored by FTIR mapping on single crystals.

To facilitate the following discussion, Figure 1 shows the amphibole crystal structure and the local cation environments involved in the process; full details on the amphibole crystal-chemistry can be found in Hawthorne (1983) and Hawthorne and Oberti (2007).

MATERIALS AND METHODS

The studied sample is a riebeckite from an alkali pegmatite from Mt. Malosa, Zomba District (Malawi); the host rock consists of centimetre-sized orthoclase with large (up to several cm long) amphibole and aegirine crystals, associated with REE- and boron-rich minerals. The amphibole was fully characterized in Susta et al. (2018), Oberti et al. (2018) and Della Ventura et al. (2018a) using Single-crystal structure Refinement (SREF), Electron Microprobe Analysis (EMPA), Laser Ablation-Inductively Coupled Plasma-Mass Spectrometry (LA-ICP-MS), FTIR, Raman and Mössbauer spectroscopies; the crystal-chemical formula is very close to the end-member composition $^{A}\square^{B}Na_2^{C}(Fe^{2+}_3Fe^{3+}_2)^{T}Si_8O_{22}^{W}(OH)_2$ (Hawthorne et al. 2012).

Isothermal heating experiments were done on both powdered and doubly-polished crystals at the Dafne-Light facility of the Frascati National Laboratories (INFN) using a Linkam 1400XY heating stage fitted on the Bruker Hyperion 3000 FTIR microscope, equipped with a 20x Schwarzschild objective, and an MCT N_2-cooled detector.

FTIR data were collected from powdered samples in conventional KBr-mineral pellets (mixed in a 7/200 weight ratio) and on pure mineral-powder pellets prepared with finely ground riebeckite pressed within a metallic die. The target temperature was reached as quickly as possible, with a heating rate of 90 °C/min, and afterword held constant. FTIR spectra were collected every 5 min, as long as the OH-stretching band was detectable.

Non-polarized single-crystal *HT*-FTIR spectra were collected on five fragments obtained by breaking a doubly polished chip of 85 μm thickness. The spot size was 100 x 100

This is the peer-reviewed, final accepted version for American Mineralogist, published by the Mineralogical Society of America.
The published version is subject to change. Cite as Authors (Year) Title. American Mineralogist, in press.
DOI: https://doi.org/10.2138/am-2022-8021. http://www.minsocam.org/

μm^2. These fragments were used for isothermal runs at 520, 530, 540, 550, 560 °C, respectively. HT-FTIR spectra were collected every minute with the same experimental set-up used for powders. All fragments were obtained from a single chip, ensuring the same thickness and crystallographic orientation (hk0) of the samples used in all five experiments.

FTIR-FPA (focal-plane-array) images were acquired at beamline B22 of the Diamond Light Source facility (Chilton, Oxfordshire, UK), using the Linkam 1400XY (T accuracy ± 1°C, according to the manufacturer) heating-stage mounted on the Bruker Hyperion 3000 FTIR microscope, equipped with a 20x Schwarzschild objective and a 64 x 64 pixel focal-plane array of detectors (FPA). The microscope was attached to a Vertex 80V optical bench equipped with a broadband KBr beamsplitter and a Globar IR source. The spectral resolution was set at 4 cm^{-1} and 16 scans were averaged for each spectrum. A 4 x 4 binning was used to reduce the acquisition time and obtain a better S/N ratio. With this configuration, each FPA frame covers a field of view of 128 µm x 128 µm with a nominal spatial resolution of ~5 µm (Della Ventura et al. 2014). The sample was heated with a rate of 90 °C/min to 520 °C and held at this temperature for 5 minutes, then it was quickly quenched and the images were collected at room-*T* by automatically moving the sample stage. The heating/cooling procedure was repeated several times, achieving a series of cumulative annealing time of 10, 20, 40, 60, 80, 100 and 140 minutes. SR-FTIR (synchrotron-radiation FTIR) spectra were acquired using a 36X Schwarzschild objective and a high-sensitivity MCT nitrogen-cooled detector. The beam size was set at 15 x 15 μm^2, with a spectral resolution of 4 cm^{-1}; 32 spectra were co-added for the sample and 128 for the background. The sample was heated rapidly to 520 °C then the temperature was kept constant and single-spot spectra were collected *in-situ* at five different positions every 5 minutes, 4 along the crystallographic *c*-axis and one in the perpendicular direction. For all types of experiment, the area of the IR absorption generated by O-H bond stretching was determined via a linear baseline correction and subsequent integration in the range 3560 – 3693 cm^{-1} using the Origin software package.

PRELIMINARY TESTS AND CHOICE OF OPERATING CONDITIONS

At the beginning of the work, different sample types and experimental conditions for the isothermal runs were tested: doubly polished single crystals heated in air or in a flow of N_2; a pellet consisting of finely ground amphibole embedded in a KBr matrix, and a pellet of pure amphibole powder. The powdered samples were both run in air. The OH-stretching intensity (for a more detailed explanation see below) was monitored for the duration of each experiment and the results are shown in Figure 2; for better comparison, the integrated

absorbance was normalized to the first value collected at the target temperature (at time 0). Both trends for single crystals show an initial increase followed by a progressive decrease in absorbance. However, the kinetic curve for the crystal heated in air (solid triangles) has a maximum near 20 min and indicates complete loss of hydroxyl groups after 90 min, whereas the crystal heated in N_2 shows a very broad kinetic curve, smeared over the entire time range and with no OH loss even after 180 min (Fig. 2, open triangles). On the other hand, the experiments on pellets show two different trends: for the pure riebeckite powder there is a rapid decrease of the OH absorbance (Fig. 2, solid squares), whereas the same powder pelletized into KBr does not deprotonate even after prolonged heating (> 180 min, Fig. 2, open squares). The implications for the trends in Figure 2 will be discussed below, however, based on these tests, the following experiments were done in air, on single-crystals and on pure mineral pellets.

ISOTHERMAL EXPERIMENTS

For isothermal-heating experiments on pure riebeckite powders, six separate runs were done at 450, 460, 470, 480, 490 and 500 °C, respectively. Figure 3a shows selected spectra collected *in situ* after 1, 5, 25, 50 and 100 minutes at a constant temperature of 470 °C. The spectrum of the untreated amphibole (Fig. 3a) consists of two main components at 3620 and 3633 cm^{-1}, which are assigned to the stretching mode of OH-groups associated with $Fe^{2+}Fe^{2+}Fe^{2+}$-OH-□ and $MgFe^{2+}Fe^{2+}$-OH-□ local arrangements, respectively (□ stands for a vacancy at the A site), plus a minor absorption at 3654 cm^{-1} that is assigned to OH-groups in the $MgMgFe^{2+}$-OH-□ arrangement (Susta et al. 2018). At high temperature, there is a shift in the position of the OH-stretching bands toward lower wavenumbers, compared to room-*T* (R*T*), due to the temperature-induced increase of the O-H bond length; the band position remained constant for the entire duration of the isothermal experiment. As required by theory, all spectra collected at 470 °C show a considerable broadening of the OH-stretching band compared to the untreated sample, due to temperature-enhanced phonon decay (e.g., Kuzmany 2009). The gradual increase in the band width over time reflects the increase of the disorder at the W site caused by the time-evolving mobilization of H^+. Due to such increasing band broadening, the three components present at R*T* are barely resolved after 50 minutes at H*T* and merge into a single band with a rounded profile. In summary, starting from the first minute at H*T* the OH-band progressively decreases in intensity and disappears after 100 minutes.

This is the peer-reviewed, final accepted version for American Mineralogist, published by the Mineralogical Society of America.
The published version is subject to change. Cite as Authors (Year) Title. American Mineralogist, in press.
DOI: https://doi.org/10.2138/am-2022-8021. http://www.minsocam.org/

Five single-crystal isothermal-heating experiments were done at 520, 530, 540, 550 and 560 °C. Figure 3b shows selected spectra collected every 10 minutes at the constant temperature of 540 °C for the 85 μm thick fragment, plotted with the same absorbance scale. The R*T* spectrum is similar to that described for the powdered sample, although component bands are slightly broader than those of the powder patterns. As crystal was thin enough to avoid artificial deformation of the signal, we may speculate that this band broadening may be related to the longer pathway of light through the single crystal. This being the case, there is a higher probability for the light to interact with intrinsic structural defects that are always present in natural samples. The initial (~1 min) H*T* spectrum in Figure 3b was collected *in situ* immediately after reaching the target temperature; as in the case of powders, it shows considerable broadening and shift in positions of the OH-stretching band with respect to the untreated sample. An interesting feature of Figure 3b is that there is a marked increase in the absorption intensity as a function of time (t): after 10 minutes it reaches its maximum, and for longer time the intensity decreases; for t > 30 min, the OH signal is barely apparent and for t = 40 min it has disappeared.

The evolution of the OH-stretching intensity over time for the isothermal experiments on powders and single crystals is shown in Figure 4a and 4b, respectively. Each pattern was normalized to the first spectrum collected at the target temperature ($A_r = 100 \cdot A_t/A_0$). Inspection of Figure 4a shows that, upon heating, for pure powders there is an exponential decrease of the O-H absorbance over time. The decrease rate is faster at higher temperatures; at 500 °C, the OH signal is halved after just 10 minutes, whereas at 450 °C, signal is halved after 50 minutes of continuous heating. The trends for single crystals (Fig. 4b), similar to what has already been shown in Figure 3b, are completely different; there is an initial increase up to 25% of the absorbance, followed by an exponential decay of the intensity for increasing heating time. The maximum increase in intensity shifts in time as a function of the temperature: at T = 540 °C it is reached after 10 minutes, while for T = 520 °C the maximum is reached after 20 minutes. At 550 °C, the increase in intensity is barely noticeable, and at very high T (560 °C) there is practically no increase.

To gather further information on the possible preferential crystallographic directions of the loss of H^+ through the amphibole, we collected several FTIR images of the OH signal using an FTIR-FPA detector on a strongly elongated single-crystal doubly polished to 136 μm thickness; the study was augmented by additional *in-situ* SR-FTIR spot measurements on a second sample. FPA images collected at RT after annealing the sample at 520°C for different times show a progressive decrease in the OH-absorbance over time (Fig. 5a); however, they

also underline that the decrease in the signal is not homogeneous throughout the sample. In fact, the crystal core retains a significant amount of OH until at least after 80 min of heating. This feature is also evident in Figure 5b where the OH absorbance at three selected points (data extracted from three pixels in the FPA image indicated in Figure 5a) is plotted against time. Whereas the signal on points close to the crystal edges (1 and 3) shows a monotonic decrease down to ~25/30% of the initial concentration, at the crystal core (point 2), the integrated absorbance remains constant up to 60 min of heating and then decreases to 50%.

In situ SR-FTIR measurements were done along transects both parallel and normal to the elongation axis of a second 147 μm thick crystal (Fig. 6). The evolution over time of the OH-absorbance measured at two positions normal to the elongation axis of the same sample is shown in Figure 6a. It is interesting to note that in the crystal core (Fig. 6a, point 1a) the absorbance trend behaves similarly to that observed in Figure 4b (i.e., an initial increase in the intensity of the signal is followed by a progressive decrease). At the crystal rim (Fig. 6a, point 1b), there is a monotonic decrease in the absorbance down to 50% after 30 min; the average intensity over these two points is constant over time (Fig. 6a, bottom). Moreover, the same trend described for point 1a is observed at all locations at the center of the crystal elongation (Fig. 6b).

KINETICS OF RIEBECKITE DEHYDROGENATION

Although much work has been done in the past, the mechanisms involved in the H*T* dehydrogenation/dehydration process in amphiboles are not yet clearly understood, and several different models have been proposed in the literature to interpret the experimental data (e.g. Addison et al. 1962b; Clark and Freeman 1967; Graham 1981; Graham et al. 1984; Brabander et al. 1995; Johnson and Fegley 2003). For isothermal solid-state reactions in minerals, general discussions of the kinetic methods can be found in Hancock and Sharp (1972) or Brown et al. (1980). For amphiboles in particular, different equations were tested to model the decomposition of tremolite by Johnson and Fegley (2003); their work has shown that the process can be treated using the formalism for first-order reactions that in solid-state is described by an exponential decay, i.e. the Avrami-Erofeev equation:

$$y = 1 - \exp\big(-f(t)\big) \text{ or } A_t = A_0 \cdot \exp\big(-f(t)\big) \qquad (2)$$

where $y = 1 - A_t/A_0$ is the fraction of H^+ loss at time = t (min), A_t is the integrated absorbance (A_i) at time = t, A_0 is A_i at time = 0, and f(t) is an exponential function (Avrami 1939). The Avrami-Erofeev equation can be also written as (Putnis et al. 1990):

$$A_t = A_0 \cdot \exp\left[-(k \cdot t)^m\right] \qquad (3)$$

A slightly different form of this equation suitable for describing dehydration in minerals has been introduced by Hancock and Sharp (1972) and Carbone et al. (2008). In equation 3, the exponential function $f(t)$ is described by two parameters k and m. The rate constant k describes the decreasing trajectory *vs.* the concentration of the reactant, while m is a factor used to model the reaction mechanism; following Hancock and Sharp (1972) $m \approx 0.5$ is typical of diffusion-controlled reactions, while $m \approx 1.0$ indicates first-order reactions.

By linearizing equation 3 and plotting the relative absorbance ($A_r = A_t/A_0$) against the ln of *time* [$\ln(-\ln A_r) = m \ln t + m \ln k$], it is possible to visually compare the dehydrogenation rates of the different experiments. Figure 7a shows this relation for the 6 isothermal experiments done on powders. Curves with the same value of m are isokinetic (Hancock and Sharp 1972), so the graphs in Figure 7a indicate that the reaction mechanism in riebeckite powders does not change within the investigated range of temperature.

The results of the heating experiments on single crystals were modelled in the same way. However, because of the initial increase in the intensity of the OH-stretching absorbance (Figure 4b), we had to choose how to define the initial time ($t = 0$) and absorbance value (A_0). The increase in absorbance of the OH-stretching band with temperature was observed in previous studies for different minerals (Radica et al. 2015 for cordierite; Della Ventura et al. 2017 for potassic-ferro-richterite; Della Ventura et al. 2018a for riebeckite) but cannot be related to an increase in the amount of OH in the sample. As discussed in Della Ventura et al. (2018a), it is due to the enhanced amplitude of the hydrogen displacement, which affects the OH-stretching mode, during H^+ delocalization for increasing T (Della Ventura et al. 2018a). Based on this hypothesis, the starting point for the curve fitting (corresponding to $t = 0$) has been shifted where the normalized absorption reverts to the starting absorbance after an initial increase. An example of the result obtained by fitting the 540 °C data set is shown in Figure 8. Interestingly, the area underneath the increase in absorbance (stippled area in Fig. 8) is related to the temperature of the experiment (inset in Fig. 8): it reduces almost linearly in the $520 < T < 540$ °C range, and disappears for $T > 550$ °C, on the verge of the dehydrogenation. Thus Figure 8 suggests that the increase in absorbance is proportional to the kinetic energy necessary to activate H^+ mobilisation.

The parameters resulting from fitting equation (2) to the experimental data on powder and single crystals are listed in Table 1. The temperature dependence of the rate constant k, as expressed by the Arrhenius equation, can be used to calculate the activation energy E_a (kJ/mol) of the process leading to loss of H^+ from the amphibole structure. The formula is:

$$k = A \cdot \exp\left(-\frac{E_a}{RT}\right) \qquad (4a)$$

that linearized becomes:

$$\ln k = \ln \mathrm{A} - E_a/RT \qquad (4b)$$

where R is the universal gas constant, T is the temperature in Kelvin, and A is the pre-exponential factor. In this equation, the activation energy represents the limiting energy barrier for the reaction to proceed, and the pre-exponential factor is interpreted as the reaction frequency (Galwey and Brown 1999).

The rate constants k from Table 1 are plotted in Arrhenius space (Fig. 9). The activation energy (E_a) (see equation 4b above) is given by the slope of the regression line through the data multiplied by R (the Boltzmann constant). For powders, the calculated E_a for the dehydrogenation/oxidation process is 159 ± 15 kJ/mol, while for single-crystals E_a is 216 ± 20 kJ/mol.

DISCUSSION

Dehydrogenation of riebeckite: powders vs. single crystals

As discussed in the introduction, the thermal treatment of riebeckite involves the oxidation of Fe^{2+} to Fe^{3+}, due to delocalization of electrons and eventual electron ejection, accompanied by H^+ loss. One of the most interesting features observed in single-crystal samples of riebeckite is that the oxidation occurring in the temperature range ~250 < T <450 °C can be reversed by quenching the experiment (Della Ventura et al., 2018a). Important structural transformations take place around and above 450°C (Oberti et al., 2018): there is a sudden contraction of the cell parameters and a rearrangement of the tetrahedral double-chain, and the oxidation is no longer reversible. Dehydrogenation was expected to occur simultaneous with $Fe^{2+} \rightarrow Fe^{3+}$ transformation as required by reaction (1). However, by combining Raman and FTIR spectroscopy, Della Ventura et al. (2018a) showed that dehydrogenation actually begins at the sample surface but is completed within the bulk of the crystal only for T > 600°C. X-ray absorption (XAS) (Della Ventura et al. 2018b) and, more recently, Raman spectroscopy (Mihailova et al. 2021), have shown that the oxidation of Fe in amphiboles precedes and triggers the loss of hydrogen.

The experiments described in the present work help to further understand key features of this process. The data in Table 1 show two different scenarios for the riebeckite powder compared to single crystals. The exponential factor m for powders varies between 0.7 and 0.8, and coupled with the linear trend in the ln/ln graph (Fig. 7a), suggests that dehydrogenation of powdered riebeckite, i.e. of small crystallites, can be modelled as a first-order reaction where

the rate of decrease in OH is a function only of the initial OH concentration in the sample. Conversely, the *m* coefficients obtained for single crystals are > 1.0, ranging between 1.02 and 1.31 (Table 1). It is reasonable to assume that the kinetic model of Hancock and Sharp (1972) developed for dehydration process in minerals can be also suitable for dehydrogenation processes, because both solid-state phenomena involve H^+ mobilization and debonding. Hence, the dehydrogenation in riebeckite cannot be considered as a purely first-order reaction where the H^+ cation simply detaches from the hydroxyl oxygen, but a combination of different processes. In other words, for samples having a lateral dimension orders of magnitude greater that the small crystallites in a powder, there is a second energy barrier to consider, namely the diffusion of H^+ through the crystal itself. This feature is reflected in the calculated activation energies (159 *vs*. 216 kJ/mol for powders and crystals, respectively) where the value for crystals incorporates both O-H bond breaking and H^+ diffusion.

Differences in activation energies between powders and crystals have been already observed in previous works (Johnson and Fegley 2003, Farver 2010). Particularly instructive is the case of tremolite examined by Johnson and Fegley (2003); the difference in activation energy between powders and crystals is very small: 456±16 kJ/mol vs. 491±18 kJ/mol, thus ≈ 8%, and almost within the experimental errors. Tremolite is an essentially Fe-free amphibole, thus the loss of H^+ from the structure cannot be locally balanced by Fe oxidation, therefore it may only occur after the disruption of the structure at very HT. The lower activation energy measured here for riebeckite thus supports the hypothesis that hydrogen diffusion occurs in combination with Fe oxidation; the latter process is greater enhanced for powders because (a) the specific surface exposed to the atmosphere is larger, and (b) the diffusion path required for the expulsion of H^+ is much shorter.

A second issue to note regarding the studied oxidation/dehydrogenation process studied is that the presence of external oxygen ($^{ex}O_2$ in equation 1) is necessary to trigger the expulsion of H^+ from the amphibole matrix in the form of H_2O molecules. This point is evident from the preliminary experiments reported in Figure 2. Comparison of the OH-absorbance trends for powdered riebeckite shows that, when incorporated into the KBr matrix, the mineral does not dehydrogenate even at temperatures higher than those used for pure powder (520 °C vs. 500 °C). A similar observation also applies to experiments on single-crystals done under different atmospheres. Again, Figure 2 compares the OH intensity during two isotherms at 520 °C; under a flow of air the dehydrogenation process takes place in the manner discussed whereas, under a flow of N_2 and up to 240 min heating, there is no

oxidation/dehydrogenation. However, a general increase in the OH-signal is evident, due to the increased in the vibrational amplitude of the O-H bond.

The anisotropy of dehydrogenation in riebeckite

The anisotropy of dehydration/dehydrogenation in silicates is a topic of primary importance, but difficult to characterize in kinetic studies. Conflicting evidence has been provided in the literature for different minerals (see Farver 2010). For amphiboles in particular, Ingrin and Blanchard (2000) have shown that for kaersutite, H^+ transport along the *c*-axis is about five times faster than along the *b*-axis while isotropic diffusion was deduced on the basis of FTIR images by Della Ventura et al. (2018a) for the same riebeckite studied here. Brabander et al. (1995) also concluded, based on SIMS analyses on oriented crystals, that OH-F interdiffusion in tremolite is isotropic.

The problem of anisotropy in riebeckite dehydrogenation is addressed in Figures 5 and 6. For the experiments shown in Figure 5, we used a strongly elongated prismatic crystal, almost one mm long and 100 μm wide, in order to improve visualization of possible preferential directions in the dehydrogenation process, i.e. either along or perpendicular to the elongation of the crystal that is parallel to the *c* crystallographic direction. Figure 5a shows that at the beginning of the experiment, the OH distribution is almost homogenous throughout the sample; a slightly higher OH concentration at the top is likely due to a change in thickness during sample preparation. After 40 min of heating the sample to 520 °C in air, it is possible to observe how the edges of the crystals lost significant amounts of OH while the crystal core is practically unaltered. This is particular evident after 80 min when the sides of the crystals are almost anhydrous but the top and bottom zones still retain significant OH. A similar conclusion can be drawn by examining the evolution of the intensities measured in situ (Fig. 6) on selected points near the core or the edge of the crystal. Indeed, the evolution of the OH intensity at point 4 is similar to that for point 1a located in the crystal core rather than at point 1b located on the lateral edge. To summarize, the imaging experiments discussed so far suggest that in riebeckite, H^+ diffusion occurs preferentially normal to the c-axis.

A second interesting feature to be noted in Figure 6 is that the analytical points located in the crystal core show an initial intensity increase followed by a decrease, similar to that observed in Figure 4b. Conversely, the spot at the edge of the crystal (point 1b) shows a monotonic decrease in absorbance. This observation strengthens the hypothesis that the excess energy (compared to powders) observed in single-crystal experiments accumulates and

may trigger H^+ diffusion across the riebeckite structure, while at the crystal edges a faster reaction occurs with the external oxygen allowing the release of protons.

Kinetic data

The data available in the literature concerning kinetic studies for hydrogen diffusion in amphiboles are listed in Table 2. They are difficult to compare because different experimental methods and analytical conditions were used; furthermore, the various studies were done on different amphibole compositions and sample types (i.e., powders *vs*. large single crystals), and both these points significantly influence the final results. Addison et al. (1962b) plotted the rate of O_2 absorbed by one gram of crocidolite (the fibrous form of riebeckite) in one hour versus the reciprocal temperature; the activation energies (E_a) derived for the oxidation process were 88 kJ/mol when using a liquid-nitrogen cold trap and 138 kJ/mol when using a carbon-dioxide cold trap. Clark and Freeman (1967) studied the dehydrogenation of crocidolite in vacuum between 589 and 651 °C by measuring the rate of weight loss and found an activation energy of 209 kJ/mol. Activation energies ranging between 67 and 104 kJ/mol were obtained by Graham et al. (1984) for various amphiboles using D-H exchange experiments. Ingrin and Blanchard (2000) determined the diffusion rate of hydrogen in single crystals of kaersutite using sequential FTIR analysis. Experiments at 600-900 °C and 0.1 MPa pressure in an atmosphere of 90%Ar:10%H_2 yielded an activation energy of 104 ± 12 kJ/mol. Brabander et al. (1995) found an activation energy of 41 KJ/mol for the F-OH interdiffusion in tremolite at 500-800 °C and 200 MPa, while a value one order of magnitude higher (> 400 KJ/mol) was obtained by Johson and Fegley (2003) as the limiting step for the decomposition of tremolite.

Inspection of Table 2 thus shows that E_a measured for the different amphiboles covers a wide range of values, from 41 kJ/mol for OH-F exchange in tremolite (Brabander et al. 1995), to almost 500 kJ/mol for the decomposition of tremolite (Johson and Fegley 2003). The activation energy represents the limiting barrier for a reaction to occur, i.e., it is related to the process that requires the most energy to overcome. The barrier can be physical (molecular diffusion through the structure), energetic (breaking/forming of bonds) or both. Simple dehydration processes, as verified for hydrated salts, usually have activation energies of the order of 150 kJ/mol or less (e.g., Brown et al. 1980), whereas the breaking of bonds and diffusion of ions through crystal structures require much higher E_a (Galwey and Brown 1999). Typical values are those for the Si diffusion in enstatite (400 kJ/mol: Fisler et al. 1997), Ca and Mg diffusion in pyroxene (360 kJ/mol: Brady and McCallister 1983). The energy to

activate the diffusion of Sr in amphiboles has been measured to be 260 kJ/mol in hornblende (Brabander and Giletti 1995), and the diffusion of oxygen in several amphiboles varies from 160 to 240 kJ/mol (Farver and Giletti 1985).

The E_a values obtained here are in line with those observed for hydrogen diffusion in previous studies of Fe-rich fibrous sodium amphiboles (Table 2). The work of Della Ventura et al. (2018a), later confirmed by X-ray absorption spectroscopy data (Della Ventura et al. 2018b; Galdenzi et al. 2018), showed that the oxidation process occurs earlier and triggers the removal of hydrogen to maintain local charge balance at the O3 oxygen. It therefore represents the rate-limiting step for the release of H^+ and, according to the data of this work, has an energy barrier of the order of 200 kJ/mole. This value matches very well the corresponding value determined by thermal gravimetry (Clark and Freeman, 1967). The activation energy of dehydrogenation is lower than that observed for breaking chemical bonds with oxygen and diffusion of cations like Ca^{2+}, Mg^{2+} or Si^{4+} through the silicate matrix (see for example Brady and McCallister 1983 for Ca and Mg in clinopyroxene) but is much higher than that measured by Brabander et al. (1995) for simple OH-F exchange in tremolite.

CONCLUSIONS AND GEOLOGICAL IMPLICATIONS

The mechanism by which H_2O is released during geological processes is a topic of considerable interest for petrological studies and for thermodynamic models of minerals and rocks stability. This is especially true for processes related to subduction, where high-temperature conditions may cause crystal-chemical reactions that significantly affect the physical properties of the rock. Hence, the development of a comprehensive crystal-chemical model for the H*T* behavior and the dehydrogenation process in amphiboles is an important goal in geology/geophysics. The results presented here fully confirm the conclusions already obtained by recent spectroscopic studies (Della Ventura et al. 2018a, b): (i) the release of H^+ from the amphibole phase is strongly dependent on the irreversible Fe^{2+}-to-Fe^{3+} exchange, which in turn occurs, for riebeckite crystals, only at $T > 550$ °C. Only above these temperatures do we observe a readjustment of amphibole structure, in particular of the geometry of the SiO_4 rings, needed to fit the smaller Fe^{3+}-O_6 octahedra and trigger the final oxidation of iron; (ii) this process occurs only in the presence of external oxygen, which interacts with the H^+ released at the mineral surface and allows formation of H_2O molecules between the mineral grains in the rock. This observation implies that oxidizing conditions are required for the amphiboles to be efficient water sources at depth. However, the work of McCammon et al. (2004) shows that oxidizing conditions prevail in the subduction zones with

respect to the rest of the mantle, thus making the amphibole effective for water recycling in these geological contexts.

The truly unique and important result of the present study is that the preferred direction of diffusion of H^+ through the mineral bulk is *perpendicular* to the slabs of SiO_4 rings and MO_6 octahedra and therefore is achieved via hopping of H^+ among different structural slabs. However, it is known that the electric conductivity of chain silicates (Tolland 1973; Schmidbauer et al. 1996) is considerably higher *parallel* to the slabs of SiO_4 rings and MO_6 octahedra and occurs via electron hopping (Hu et al. 2018; Mihailova er al. 2021). Therefore, although the H^+ diffusion may contribute to the overall anisotropic conductivity of the amphiboles, our results suggest that ionic and electronic diffusion are not coupled.

Based on the evolution of IR absorption intensities, we show that the activation energy needed for detaching H^+ from the riebeckite structure is 150 kJ/mol for powders and 216 kJ/mol for single crystals, in good agreement with thermogravimetric studies (Clark and Freeman 1967). Furthermore, our data show that an initial phase of heat accumulation within the mineral bulk, followed by additional heat for diffusion of H^+ toward the grain surface, is required to trigger its release from the structure. So far, this phenomenon has been neglected in all models that simulate the kinetics of H^+ diffusion, probably because most of the experiments have been done on powders. However, hydrated Fe-silicates in rocks occur predominantly in the form of single crystals often of considerable size, therefore the existing kinetic models should be reevaluated to better describe trends such as those in Figure 4b, demonstrating that an additional energy is accumulated into enhanced H^+ dynamic displacements before hydrogen debonding from oxygen.

ACKNOWLEDGEMENTS. GDV was supported by the Grant to Department of Science, Roma Tre University (MIUR-Italy Dipartimenti di Eccellenza, ARTICOLO 1, COMMI 314 – 337 LEGGE 232/2016). B.M. acknowledges financial support by the Deutsche Forschungsgemeinschaft (project MI 1127/7-2). The experiment at the MIRIAM beamline B22 of Diamond were supported by beamtime SM11425.

REFERENCES

Addison C.C., Addison W.E., Neal G.H., Sharp J.H. (1962a) Amphiboles. Part I. The oxidation of crocidolite. Journal of the Chemical Society, 1468-1471.

Addison W.E., Neal G.H., Sharp J.H. (1962b) Amphiboles. Part II. The kinetics of oxidation of crocidolite. Journal of the Chemical Society, 1472-1475.

Addison W.E., Sharp J.H. (1962a) Amphiboles. Part III. The reduction of crocidolite. Journal of the Chemical Society, 3693-3698.

Addison W.E., Sharp J.H. (1962b) A mechanism for the oxidation of ferrous iron in hydroxylated silicates. Meeting of the Clay Minerals Group of the Mineralogical Society, Leeds, April 1962. 73-79.

Addison W.E., White A.D. (1968) The oxidation of Bolivian crocidolite. Mineralogical Magazine, 36, 791-796.

Avrami M. (1939). Kinetics of Phase Change. I. General Theory. Journal of Chemical Physics, 7, 1103-1112.

Barnes V.E. (1930) Changes in hornblende at about 800 °C. American Mineralogist, 15, 393-417.

Biedermann A.R., Bender Koch C., Pettke T., Hirt A.M. (2015) Magnetic anisotropy in natural amphibole crystals. American Mineralogist, 100, 1940-1951.

Brabander D.J., Hervig R.L., Jenkins D.M. (1995) Experimental determination of F-OH interdiffusion in tremolite and significance to fluorine-zoned amphiboles. Geochimica and Cosmochimica Acta 59, 3549-3560.

Brabander D.J., Giletti B.J. (1995) Strontium diffusion kinetics in in amphiboles and significance to thermal history determinations. Geochimica and Cosmochimica Acta 59, 2223-2238.

Brady J.B., McCallister R.H. (1983) Diffusion data for clinopyroxenes from homogenization and self-diffusion experiments. American Mineralogist, 68, 95-105.

Brown M.E., Dollimore D., Galwey A.K. (1980) Reactions in the solid state. Elsevier, Amsterdam.

Carbone M., Ballirano P., Caminiti R. (2008) Kinetics of gypsum dehydration at reduced pressure: an energy dispersive X-ray diffraction study. European Journal of Mineralogy, 20, 621-627.

Carlslaw H.S., Jeager J.C. (1959) Conduction of heat in solids. Oxford University Press.

Christensen N.I., Mooney W.D. (1995) Seismic velocity structure and composition of the continental crust: a global view. Journal of Geophysical Research Solid Earth 100, 9761-9788.

Clark M.W., Freeman A.G. (1967) Kinetics and mechanism of dihydroxylation of crocidolite. Transaction Faraday Society 63, 2051-2056.

Crank J. (1975) The mathematics of diffusion. Oxford University Press.

Deer W.A., Howie R.A., Zussman J. (1997) Double-chain silicates (second edition). The Geological Society, London.

Della Ventura, G., Iezzi, G., Redhammer, G.J., Hawthorne, F.C., Scaillet, B., Novembre, D. (2005) Synthesis and crystal-chemistry of alkali amphiboles in the system Na_2O-MgO-FeO-Fe_2O_3-SiO_2-H_2O as a function of f_{O2}. American Mineralogist, 90, 1375-1383.

Della Ventura G., Marcelli A., Bellatreccia F. (2014) SR-FTIR microscopy and FTIR imaging in the Earth Sciences. In Henderson GS, Neuville DR, Downs RT (eds) Spectroscopic methods in Mineralogy and Materials Sciences, Reviews in Mineralogy and Geochemistry 78, Mineralogical Society of America, Chantilly, Virginia, pp 447-479.

Della Ventura G., Susta U., Bellatreccia F., Marcelli A., Redhammer G., Oberti R. (2017) Deprotonation of Fe-dominant amphiboles: Single-crystal HT-FTIR spectroscopic studies of synthetic potassic-ferro-richterite. American Mineralogist, 102, 117-125.

Della Ventura G., Milahova B., Susta U., Cestelli Guidi M., Marcelli A., Schlüter J., Oberti R. (2018a) The dynamics of Fe oxydation in riebeckite: a model for amphiboles. American Mineralogist, 103, 1103-1111.

Della Ventura G., Galdenzi F., Cibin G., Wei X., Macis S., Marcelli A. (2018b) Iron oxidation dynamics vs. temperature of synthetic potassic-ferro-richterite: a XANES investigation. Physical Chemistry and Chemical Physics 20, 21764-21771.

Ernst W.G. (1962) Synthesis, stability relations, and occurrence of riebeckite and riebeckite-arfvedsonite solid solutions. Journal of Geology, 70, 689-736.

Ernst W.G., Wai M. (1970) Mössbauer, infrared, X-ray and optical study of cation ordering and dehydrogenation in natural and heat-treated sodic amphiboles. American Mineralogist, 55, 1226-1258.

Evans B.W. (2007) The synthesis and stability of some end-member amphiboles. In Hawthorne F.C., Oberti R., Della Ventura G., Mottana A. (eds) Amphiboles: Crystal Chemistry, Occurrence, and Health Issues, Reviews in Mineralogy and Geochemistry 67, Mineralogical Society of America, Chantilly, Virginia, pp 261-286.

Farver J.R. (2010) Oxygen and Hydrogen Diffusion in Minerals, In Zhang Y., Cherniak D.J. (eds) Diffusion in Minerals and Melts, Reviews in Mineralogy and Geochemistry 72, 447-507.

Farver J.R., Giletti B.J. (1985) Oxygen diffusion in amphiboles. Geochimica and Cosmochimica Acta 49, 1403-1411.

Fisler D.K., Mackwell S.J., Petschl S. (1997) Grain boundary diffusion in in enstatite. Physics and Chemistry of Minerals, 24, 264-273.

Galdenzi F., Della Ventura G., Cibin G., Macis S., Marcelli A. (2018) Accurate Fe^{3+}/Fe_{tot} ratio from XAS spectra at the Fe K-edge. Radiation Physics and Chemistry, https://doi.org/10.1016/j.radphyschem.2018.12.008

Galwey A.K., Brown M.E. (1999) Thermal decomposition of ionic solids. Elsevier, Amsterdam.

Ganzhorn A.C., Pilorgé H., Le Floch S., Montagnac G., Cardon H., Reynard B. (2018) Deuterium-hydrogen inter-diffusion in chlorite. Chemical Geology, 493, 518-524.

Graham C.M. (1981). Experimental hydrogen isotope studies III: Diffusion of hydrogen in hydrous minerals, and stable isotope exchange in metamorphic rocks. Contribution to Mineralogy and Petrology, 76, 216-228.

Graham C.M., Harmon R.S., Sheppard S.M.F. (1984) Experimental hydrogen isotope studies: hydrogen isotope exchange between amphibole and water. American Mineralogist, 69, 128-138.

Hancock J.D., Sharp J.H. (1972) Method of comparing solid-state kinetic data and its application to the decomposition of kaolinite, brucite, and $BaCO_3$. Journal of American Ceramic Society, 55, 74-77.

Hawthorne F.C. (1983) The crystal chemistry of the amphiboles. Canadian Mineralogist, 21, 173-480.

Hawthorne F.C., Oberti R. (2007) Amphiboles: crystal chemistry. In Hawthorne F.C., Oberti R., Della Ventura G., Mottana A. (eds) Amphiboles: Crystal Chemistry, Occurrence, and Health Issues, Reviews in Mineralogy and Geochemistry 67, Mineralogical Society of America, Chantilly, Virginia, pp 1-54.

Hawthorne F.C., Oberti R., Harlow G.E., Maresch W.V., Martin R.F., Schumacher J.C., Welch M.D. (2012) Nomenclature of the amphibole supergroup. American Mineralogist, 97, 2031-2048.

Hodgson A.A., Freeman A.G., Taylor H.F.V. (1965) The thermal decomposition of crocidolite from Koegas, South Africa. Mineralogical Magazine, 35, 5-29.

Hu H., Dai L., Heping L., Sung W., Lai B. (2018) Effect of dehydrogenation on the electrical conductivity of Fe-bearing amphibole: Implications for high conductivity anomalies in subduction zones and continental crust. Earth and Planetary Science Letters, 498, 27-37.

Ingrin J., Blanchard M. (2000) Hydrogen mobility in single crystal kaersutite. EMPG VIII, Journal of Conference Abstracts 5:52.

Johnson N.M., Fegley B. (2003) Tremolite decomposition on Venus II. Products, kinetics, and mechanism. Icarus 164, 317-333.

King P.L., Hervig R.L., Holloway J.R., Vennemann T.W., Righter K. (1999) Oxy-substitution and dehydrogenation in mantle-derived amphibole megacrysts. Geochimica and Cosmochimica Acta 63, 3635-3651.

King P.L., Hervig R.L., Holloway J.R., Delaney J.S., Dyar M.D. (2000) Partitioning of Fe^{3+}/Fe_{total} between amphibole and basanitic melt as a function of oxygen fugacity. Earth and Planetary Science Letters 178, 97-112.

Kuzmany H. (2009) Solid state spectroscopy: an introduction. Springer-Verlag, Berlin.

Manthilake G., Bolfan-Casanova N., Novella D., Mookherjee M., Andrault D. (2016) Dehydration of chlorite explains anomalously high electrical conductivity in the mantle wedges. Science Advances 2, e1501631, DOI:10.1126/sciadv.1501631

McCammon C.A., Frost D.J., Smyth J.R., Laustsen H.M.S., Kawamoto T., Ross N.L., van Aken P.A. (2004) Oxidation state of iron in hydrous mantle phases: implications for subduction and mantle oxygen fugacity. Physics of the Earth and Planetary Interiors, 143-144, 157-169.

Mihailova B., Della Ventura G., Waeselmann N., Wei Xu, Schlüter J., Galdenzi F., Marcelli A., Redhammer G.J., Boiocchi M., Oberti R. (2021) Coupled phonon-electron excitations in hydrous Fe-bearing silicates: a key to understanding lithospheric conductivity. Communication Materials, in press.

Momma K., Izumi F. (2008) VESTA: a three-dimensional visulization system for electronic and structural analysis. Journal of Applied Crystallography, 41, 653-658.

Moukarika A., Coey J.M.D., Dang N.V. (1983) Magnetic order in crocidolite asbestos. Physics and Chemistry of Minerals 9, 269-275.

Oberti R., Della Ventura G., Cámara F. (2007) New amphibole compositions: natural and synthetic. In Hawthorne F.C., Oberti R., Della Ventura G., Mottana A. (eds). Amphiboles: Crystal Chemistry, Occurrence, and Health Issues, Reviews in Mineralogy and Geochemistry 67, Mineralogical Society of America, Chantilly, Virginia, pp 89-123.

Oberti R., Boiocchi M., Zema M., Della Ventura G. (2016) Synthetic potassic-ferro-richterite: 1. Composition, crystal structure refinement and H*T* behavior by in operando single-crystal X-ray diffraction. Canadian Mineralogist, 54, 353-369.

Oberti R., Boiocchi M., Zema M., Hawthorne F.C., Redhammer G.J., Susta U., Della Ventura G. (2018) Understanding the peculiar HT behavior of riebeckite: espansivity, deprotonation, Fe-oxidation and a novel cation disorder scheme. European Journal of Mineralogy, 3, 437-449.

Oberti R., Boiocchi M., Zema M. (2019) Thermoelasticity, cation exchange, and deprotonation in Fe-rich holmquistite: toward a crystal-chemical model for the high-temperature behavior of orthorhombic amphiboles. American Mineralogist, 104, 1829-1839.

Patterson J.H. (1964) The thermal disintegration of crocidolite in air and in vacuum. Mineralogical Magazine, 35, 31-37.

Phillips M.W., Popp R.K., Clowe C.A. (1988) Structural adjustments accompanying oxidation-dehydrogenation in amphiboles. American Mineralogist, 73, 500-506.

Phillips M.W., Draheim J.E., Popp R.K., Clowe C.A., Pinkerton A.A. (1989) Effect of oxidation-dehydrogenation in tschermakitic hornblende. American Mineralogist, 74, 764-773.

Phillips M.W., Popp R.K., Clowe C.A. (1991) A structural investigation of oxidation effects in air-heated grunerite. American Mineralogist, 76, 1502-1509.

Popp R.K., Virgo D., Yoder H.S., Hoering T.C., Phillips M.W. (1995) An experimental study of phase equilibria and Fe oxy-component in kaersutitic amphibole: implications for the f_{H2} and a_{H2O} in the upper mantle. American Mineralogist, 80, 534–548.

Putnis A., Winkler B., Fernandez-Diaz L. (1990) In situ IR spectroscopic and thermogravimetric study of the dehydration of gypsum. Mineralogical Magazine, 54, 123-128.

Radica F., Della Ventura G., Bellatreccia F., Cestelli Guidi M. (2015) HT-FTIR micro-spectroscopy of cordierite: the CO_2 absorbance from in situ and quench experiments. Physics and Chemistry in Minerals, 43, 69 – 81, DOI 10.1007/s00269-015-0775-4.

Radica F., Della Ventura G., Bellatreccia F., Cinque G., Cestelli Guidi M. (2016) The diffusion kinetics of CO_2 in cordierite: an H*T*-FTIR micro-spectroscopy study. Contribution to Mineralogy and Petrology, 171, 12, DOI 10.1007/s00410-016-1228-x

Robb L. (2005) Introduction to ore-forming processes. Blackwell Malden, USA.

Rouxhet P.G., Gillard J.L., Fripiat J.J. (1972) Thermal decomposition of amosite, crocidolite and biotite. Mineralogical Magazine, 38, 583-592.

Saltas V., Pentari D., Vallianatos F. (2020) Complex electrical conductivity of biotite and muscovite micas at elevated temperatures: a comparative study. Materials 13, 3513, DOI 10.3390/ma13163513

Schmidbauer E., Kunzmann Th., Fehr Th., Hochleitner R. (1996) Electrical conductivity, thermopower and ^{57}Fe Mössbauer spectroscopy on an Fe-rich amphibole, arfvedsonite. Physics and Chemistry of Minerals, 23, 99-106.

Schmidbauer E., Kunzmann Th., Fehr Th., Hochleitner R. (2000) Electrical resistivity and ^{57}Fe Mossbauer spectra of Fe-bearing calcic amphiboles. Physics and Chemistry of Minerals, 27, 347-356.

Shankland T.J. Ander M.E. (1983) Electrical conductivity, temperatures, and fluids in the lower crust. Journal of Geophysical Research, 88, 9475-9484.

Schmidt M.W., Poli S. (1998) Experimentally based water budgets for dehydrating slabs and consequences for arc magma generation. Earth and Planetary Science Letters, 163, 361-379.

Susta U., Della Ventura G., Hawthorne F.C., Abdu Y.A., Day M.C., Mihailova B., Oberti R. (2018) The crystal-chemistry of riebeckite, ideally $Na_2Fe^{2+}{}_3Fe^{3+}{}_2Si_8O_{22}(OH)_2$: a multidisciplinary study. Mineralogical Magazine, 82, 837-852

Tokiwai K., Nakashima S. (2010). Dehydration kinetics of muscovite by in situ infrared microspectroscopy. Physics and Chemistry of Minerals, 37, 91-101.

Tolland H. (1973) Mantle conductivity and electrical properties of garnet, mica and amphibole. Nature 241:35-36.

Ungaretti L. (1980) Recent developments in X-ray single crystal diffractometry applied to the crystal-chemical study of amphiboles. Godisnjak Jugonslavenskog Centra za Kristalografiju, 15:29-65.

Zhou W., Fan D., Liu Y., Xie H. (2011) Measurements of wave velocity and electrical conductivity of an amphibolite from southwestern margin of the Tarim basin at pressures to 1.0 GPa and temperatures to 700 °C: comparison with field observations. Geophysics Journal International, 187, 1393-1404.

Wang D., Guo Y., Yu Y., Karato S. (2012). Electrical conductivity of amphibole-bearing rocks: influence of dehydration. Contribution to Mineralogy and Petrology, 164, 17–25.

Welch M.D., Cámara F., Della Ventura G., Iezzi G. (2007) Non-ambient in situ studies of amphiboles. In Hawthorne FC, Oberti R, Della Ventura G, Mottana A (eds)

Amphiboles: Crystal Chemistry, Occurrence, and Health Issues, Reviews in Mineralogy and Geochemistry 67, Mineralogical Society of America, Chantilly, Virginia, pp 223-260.

Table 1. Fitting parameters obtained using the Avrami equation (eq. 3, see text) for the isothermal experiments performed on pure powders and doubly polished single crystals. The uncertainty in the last digit is given in brackets.

Temperature (°C)	**Sample type**	***k***	***m***	**-log *k***
450	Powder	0.0119 (3)	0.81 (3)	4.43 (2)
460	Powder	0.0141 (3)	0.76 (3)	4.26 (1)
470	Powder	0.0220 (4)	0.75 (2)	3.81 (1)
480	Powder	0.027 (1)	0.78 (3)	3.62 (2)
490	Powder	0.043 (1)	0.70 (2)	3.15 (1)
500	Powder	0.071 (2)	0.74 (3)	2.64 (2)
520	Single crystal	0.0493 (3)	1.31 (1)	3.01 (1)
530	Single crystal	0.074 (1)	1.11 (2)	2.60 (1)
540	Single crystal	0.132 (1)	1.02 (2)	2.60 (1)
550	Single crystal	0.196 (4)	1.17 (4)	1.63 (2)
560	Single crystal	0.204 (2)	1.28 (3)	1.59 (1)

This is the peer-reviewed, final accepted version for American Mineralogist, published by the Mineralogical Society of America.
The published version is subject to change. Cite as Authors (Year) Title. American Mineralogist, in press.
DOI: https://doi.org/10.2138/am-2022-8021. http://www.minsocam.org/

Table 2. Kinetic and diffusion parameters reported in the literature for amphiboles.

Sample	Sample type	Process	E_a (KJ/mol)	$\log D_0$ (D_0 in m^2/s)	Reference
Tremolite	powder	H^+ diffusion	71.5	-10.7	Graham et al. (1984)
Tremolite	crystal	F-OH exchange	41	-16.5	Brabander et al. (1995)
Tremolite	powder	Decomposition	456	n.a.	Johnson and Fegley (2000)
Tremolite	crystal	Decomposition	491	n.a	Johnson and Fegley (2000)
Actinolite	powder	H^+ diffusion	99	-9.2	Graham et al. 1984
Actinolite	powder	H^+ diffusion	102	-7.6	Suzuoki and Epstein (1976)
Pargasitic	crystal	OH-Cl exchange	106	-9.3	Su et al. (2014)
Kaersutite	crystal	H^+ diffusion	104	-8.7	Ingrind and Blanchard (2000)
Horneblende	powder	H^+ diffusion	79-84	-11.6	Graham et al. (1984)
Riebeckite	fibre	Oxydation	88-138	n.a.	Addison et al. (1962)
Riebeckite	crystal	OH/decomp	204	n.a.	Clark and Freemam (1967)
Riebeckite	powder	Dehydrogenation	159±15	n.a.	this work
Riebeckite	crystal	Dehydrogenation	216±20	n.a.	this work

This is the peer-reviewed, final accepted version for American Mineralogist, published by the Mineralogical Society of America.
The published version is subject to change. Cite as Authors (Year) Title. American Mineralogist, in press.
DOI: https://doi.org/10.2138/am-2022-8021. http://www.minsocam.org/

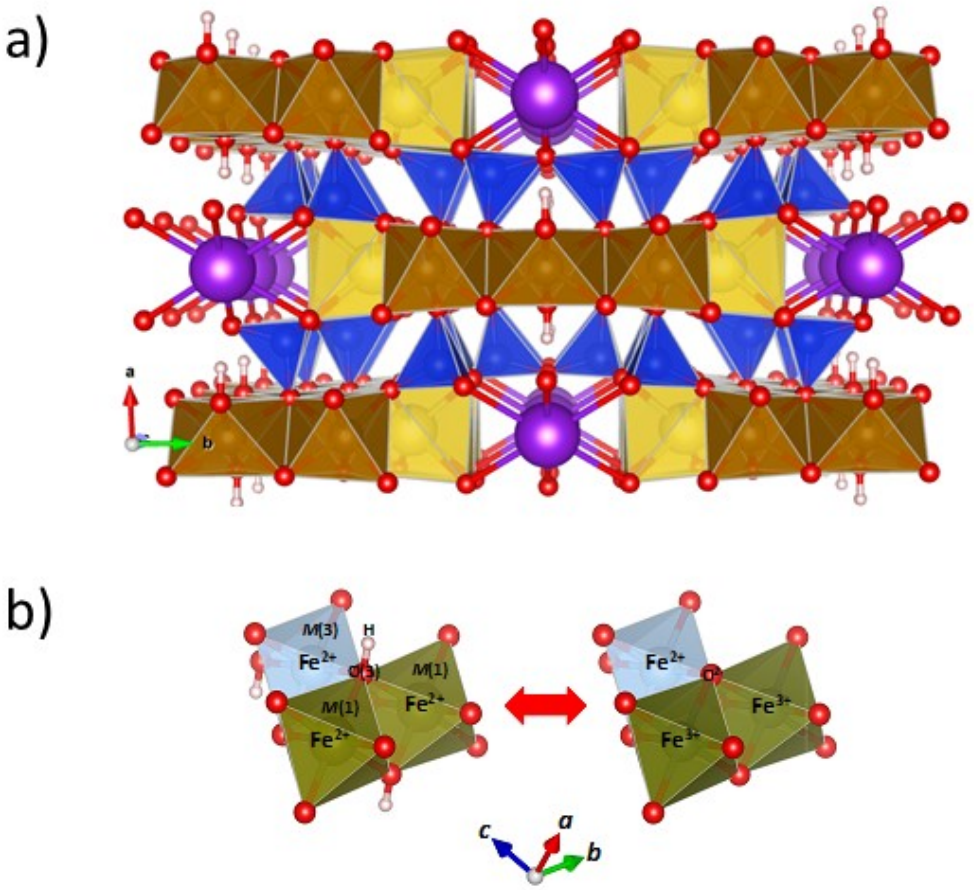

Figure 1. (a) The structure of monoclinic amphiboles (*C*2/*m*) projected along the c axis. Brown: *M*(1-2-3) sites, yellow: *M*(4) site, purple: *A*-site, blue: tetrahedral sites. The red spheres represent the oxygen atoms and the white spheres are the hydrogen atoms connected to the O3 oxygen. (b) schematic local modification of the O3 environment during the oxidation/dihydroxylation.

This is the peer-reviewed, final accepted version for American Mineralogist, published by the Mineralogical Society of America.
The published version is subject to change. Cite as Authors (Year) Title. American Mineralogist, in press.
DOI: https://doi.org/10.2138/am-2022-8021. http://www.minsocam.org/

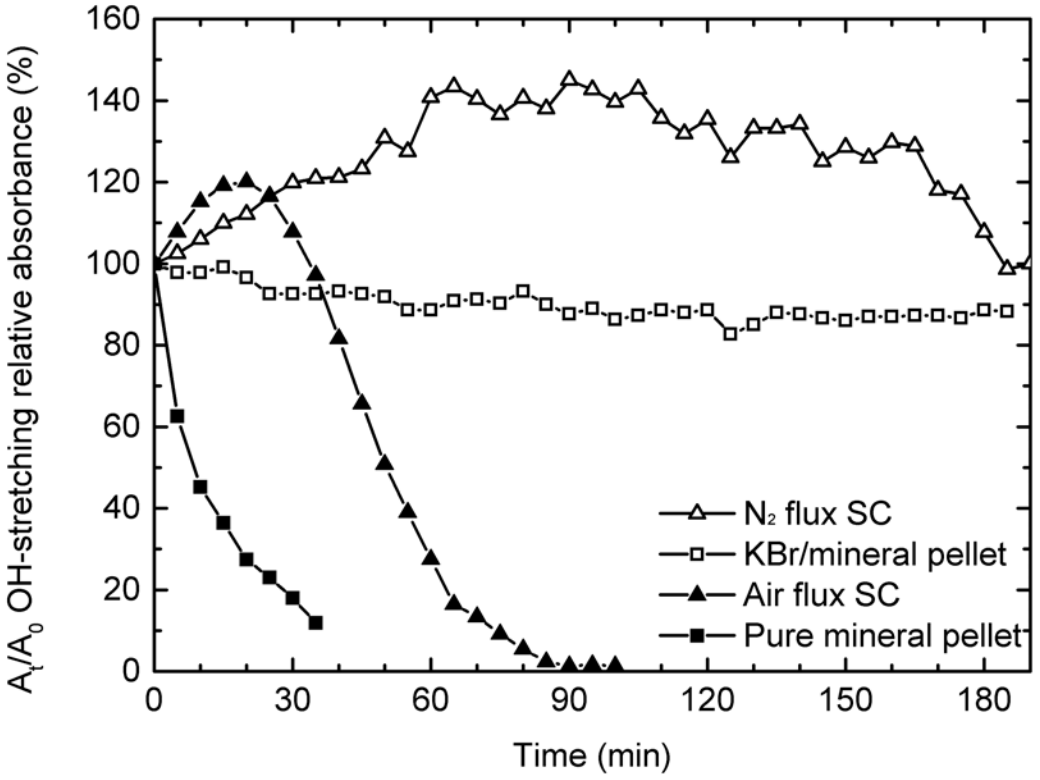

Figure 2. OH-stretching relative absorbance (A_t/A_0 in %) for different sample types and atmospheres (see text for explanation) derived from isothermal experiments conducted at 520 °C except for the pure mineral pellet, which was done at 500 °C. SC = single crystal.

This is the peer-reviewed, final accepted version for American Mineralogist, published by the Mineralogical Society of America.
The published version is subject to change. Cite as Authors (Year) Title. American Mineralogist, in press.
DOI: https://doi.org/10.2138/am-2022-8021. http://www.minsocam.org/

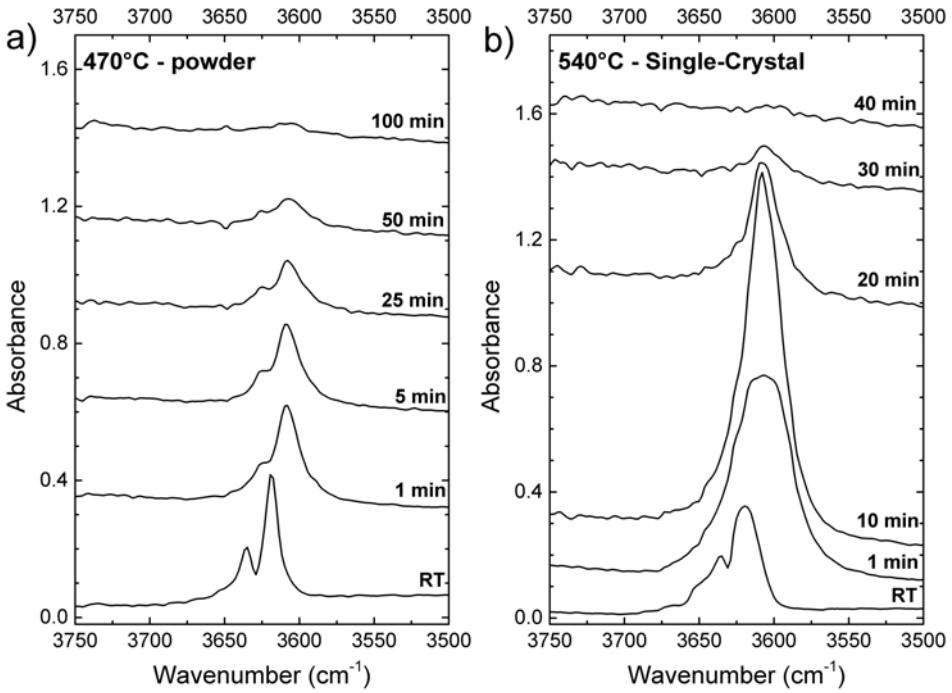

Figure 3. Selected OH-stretching spectra measured *in situ* at 470° C on pure powders (a) and at 540°C on a doubly polished 85 μm thick section (b). Spectra are plotted with the same absorbance scale. The spectrum collected at room *T* (R*T*) is also provided.

This is the peer-reviewed, final accepted version for American Mineralogist, published by the Mineralogical Society of America.
The published version is subject to change. Cite as Authors (Year) Title. American Mineralogist, in press.
DOI: https://doi.org/10.2138/am-2022-8021. http://www.minsocam.org/

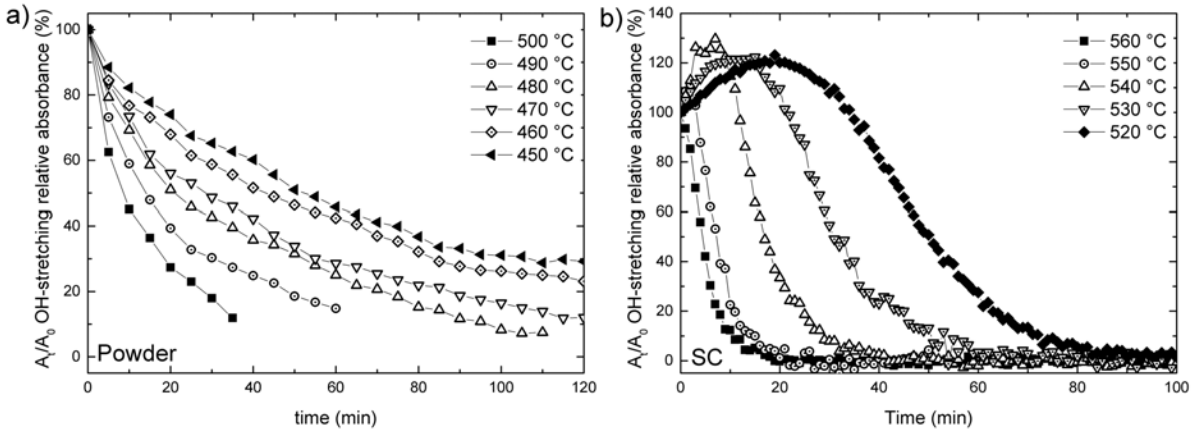

Figure 4. OH-stretching relative absorbance (A_t/A_0 in %) as a function of time during isothermal experiments on (a) pure powder pellets and (b) on a doubly polished, 85 μm-thick, single-crystal (b). Integration range is 3711-3560 cm^{-1}.

This is the peer-reviewed, final accepted version for American Mineralogist, published by the Mineralogical Society of America.
The published version is subject to change. Cite as Authors (Year) Title. American Mineralogist, in press.
DOI: https://doi.org/10.2138/am-2022-8021. http://www.minsocam.org/

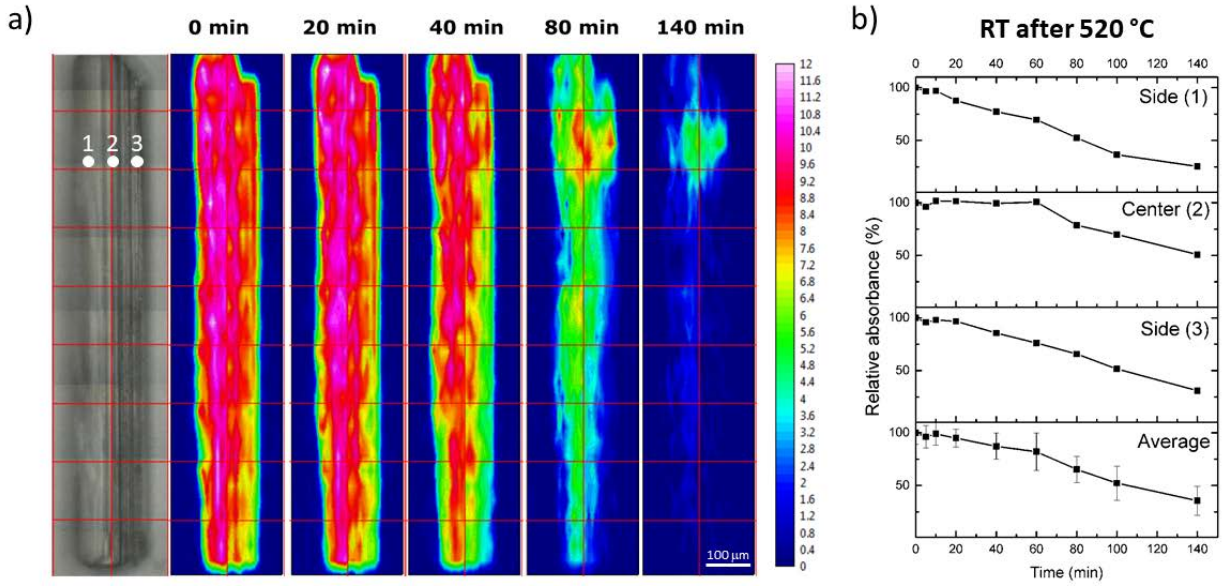

Figure 5. (a) Infrared images collected with an FPA detector at RT after quenching the sample heated at 520°C for the cumulative time indicated. Doubly polished prismatic crystal, 136 µm thick. Left: optical image of the studied crystal; right: OH-absorbance scale. (b) Trends in absorbance over time for three selected points (1,2 and 3) perpendicular to the *c*-axis as extracted from the FPA images. The absorbance values were calculated by integrating the 3693-3560 cm^{-1} range.

This is the peer-reviewed, final accepted version for American Mineralogist, published by the Mineralogical Society of America.
The published version is subject to change. Cite as Authors (Year) Title. American Mineralogist, in press.
DOI: https://doi.org/10.2138/am-2022-8021. http://www.minsocam.org/

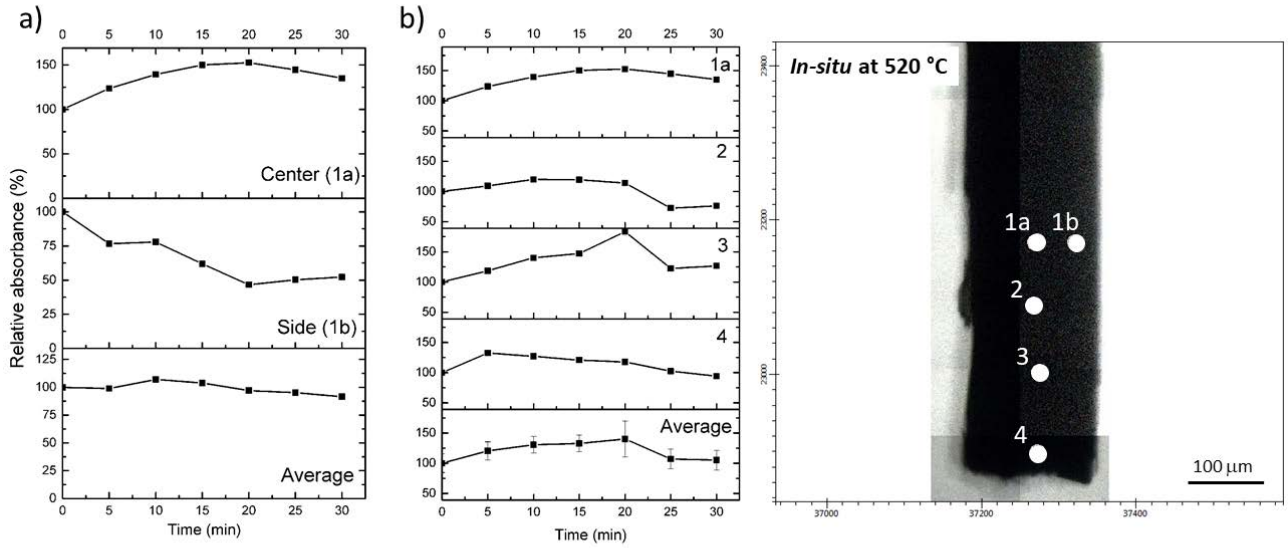

Figure 6. *In situ* absorbance as a function of time for a set of points numbered on the figure and chosen along (a) the longitudinal and (b) perpendicular direction of a doubly polished crystal, 147 µm-thick (right). A synchrotron FTIR beam was used with a spot 15 x 15 μm^2. Absorbance values are calculated by integrating the 3693-3560 cm^{-1} range.

This is the peer-reviewed, final accepted version for American Mineralogist, published by the Mineralogical Society of America.
The published version is subject to change. Cite as Authors (Year) Title. American Mineralogist, in press.
DOI: https://doi.org/10.2138/am-2022-8021. http://www.minsocam.org/

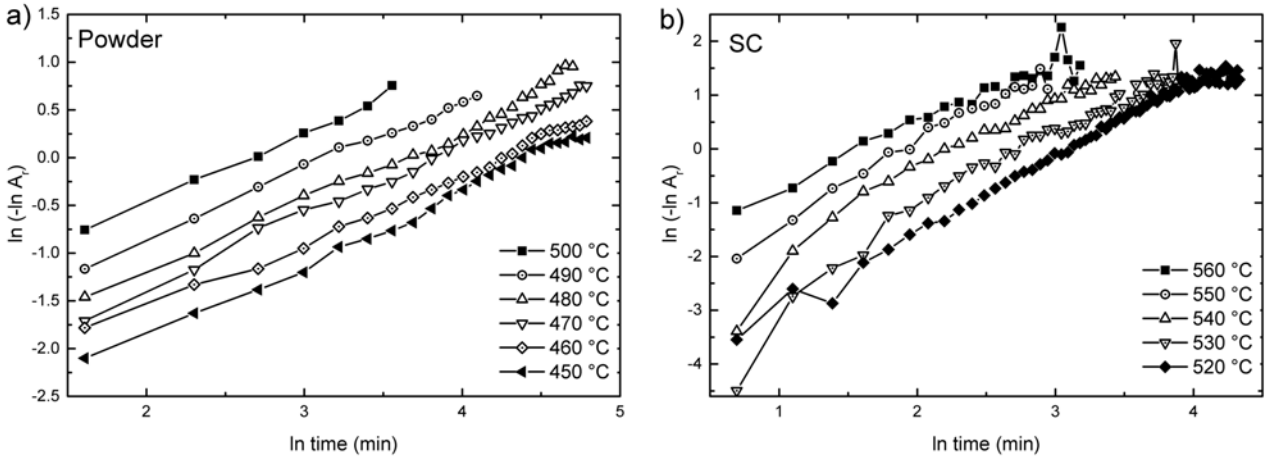

Figure 7. Plot of ln(-ln A_r) versus ln of time for dehydration experiments on powders (a) and single-crystals (b); A_r is the relative absorbance (A_t/A_0).

This is the peer-reviewed, final accepted version for American Mineralogist, published by the Mineralogical Society of America.
The published version is subject to change. Cite as Authors (Year) Title. American Mineralogist, in press.
DOI: https://doi.org/10.2138/am-2022-8021. http://www.minsocam.org/

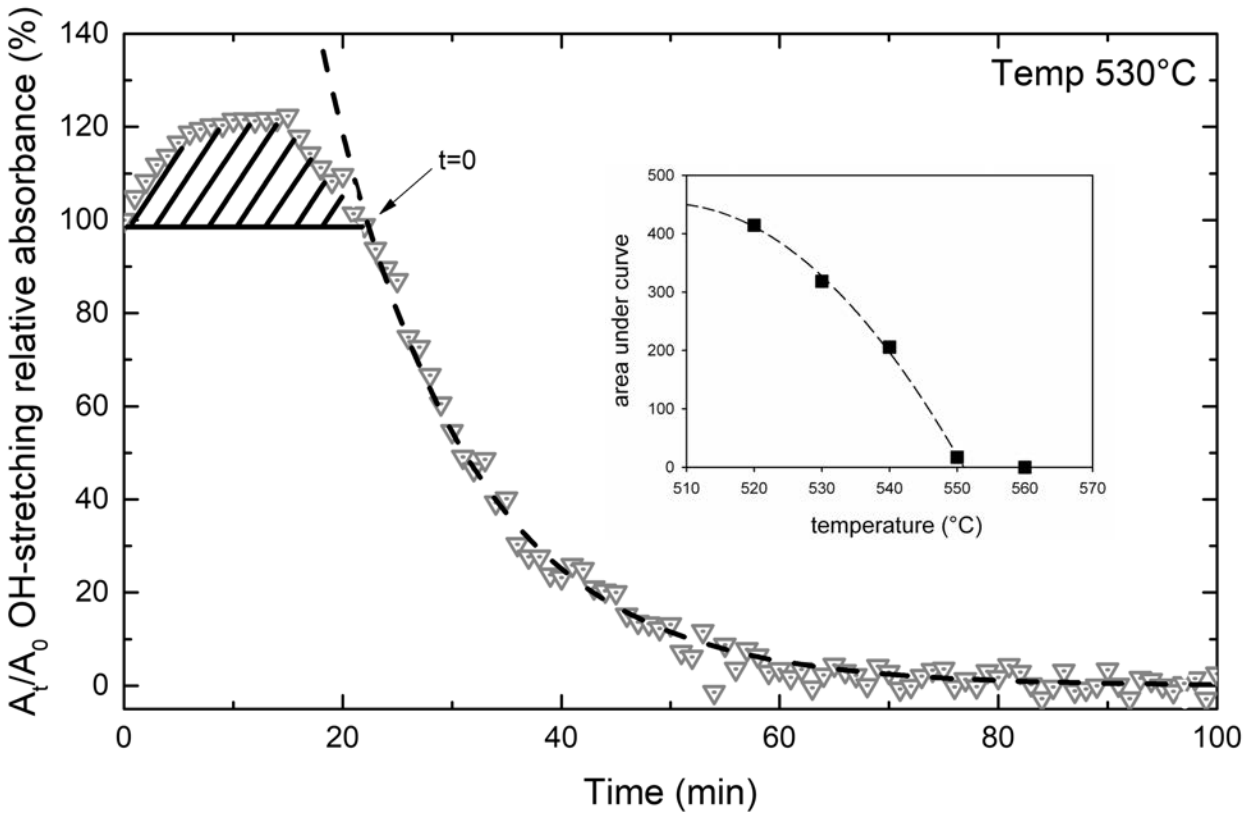

Figure 8. Example of the procedure used to set the t = 0 point to model data collected on single crystals at different temperatures (see text for an explanation). The resulting fit for the data collected at 540° C is shown (dashed line) as an example. The stippled area denotes the increase in intensity. The inset shows the relation between the stippled areas versus temperature for the different experiments.

This is the peer-reviewed, final accepted version for American Mineralogist, published by the Mineralogical Society of America.
The published version is subject to change. Cite as Authors (Year) Title. American Mineralogist, in press.
DOI: https://doi.org/10.2138/am-2022-8021. http://www.minsocam.org/

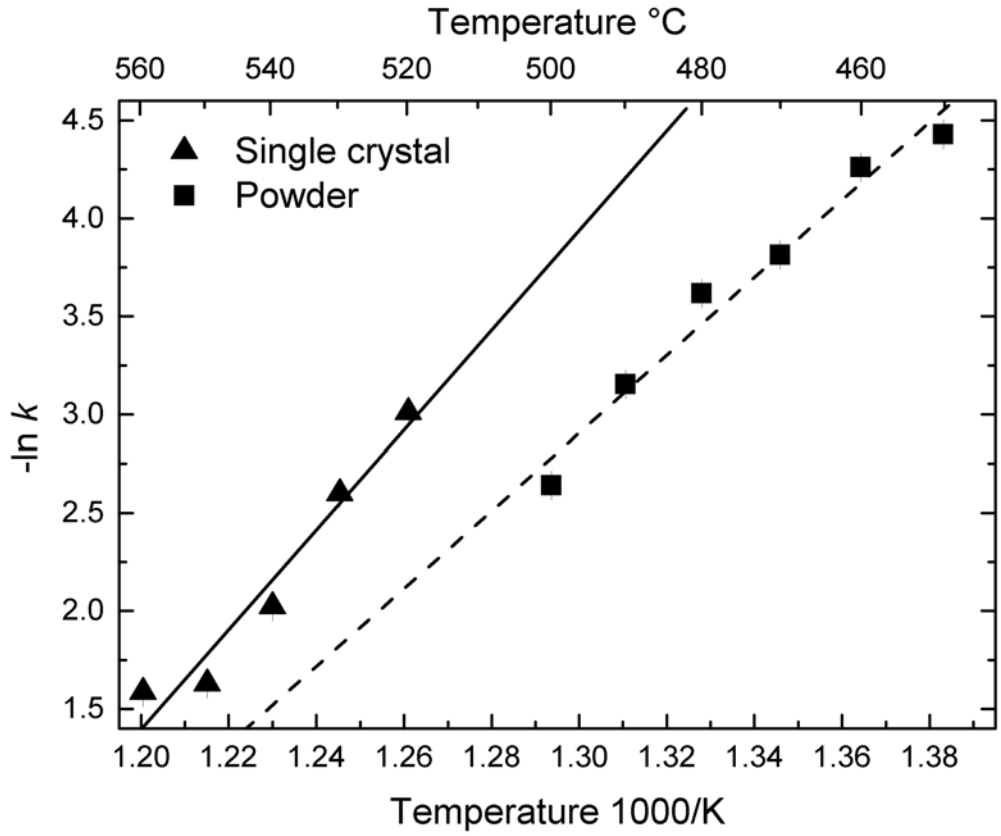

Figure 9. Arrhenius plot for the kinetic data obtained on powders and single crystals. Error bars are smaller than the symbol.